J|A|C|S
ARTICLES
Published on Web 10/24/2006

Characterization of the Phenoxyl Radical in Model Complexes for the Cu_B Site of Cytochrome *c* Oxidase: Steady-State and Transient Absorption Measurements, UV Resonance Raman Spectroscopy, EPR Spectroscopy, and DFT Calculations for M-BIAIP

Yasutomo Nagano,[†] Jin-Gang Liu,[‡] Yoshinori Naruta,*[,†] Tadaaki Ikoma,[§] Shozo Tero-Kubota,[§] and Teizo Kitagawa*[,†]

Contribution from the Okazaki Institute for Integrative Bioscience, National Institutes of Natural Science, Okazaki 444-8787, Japan, Institute for Materials Chemistry and Engineering, Kyusyu University, Fukuoka 812-8581, Japan, and Institute of Multidisciplinary Research for Advanced Materials, Tohoku University, Sendai 980-8577, Japan

Received March 3, 2006; E-mail: naruta@ms.ifoc.kyushu-u.ac.jp; teizo@ims.ac.jp

Abstract: Physicochemical properties of the covalently cross-linked tyrosine-histidine-Cu_B (Tyr-His-Cu_B) unit, which is a minimal model complex [M^{II}-**BIAIP**Br]Br (M = Cu^{II}, Zn^{II}) for the Cu_B site of cytochrome *c* oxidase, were investigated with steady-state and transient absorption measurements, UV resonance Raman (UVRR) spectroscopy, X-band continuous-wave electron paramagnetic resonance (EPR) spectroscopy, and DFT calculations. The pH dependency of the absorption spectra reveals that the pK_a of the phenolic hydroxyl is ca. 10 for the Cu^{II} model complex (Cu^{II}-**BIAIP**) in the ground state, which is similar to that of *p*-cresol (tyrosine), contrary to expectations. The bond between Cu^{II} and nitrogen of cross-linked imidazole cleaves at pH 4.9. We have successfully obtained UVRR spectra of the phenoxyl radical form of **BIAIP**s and have assigned bands based on the previously reported isotope shifts of Im-Ph (2-(1-imidazoyl)-4-methylphenol) (Aki, M.; Ogura, T.; Naruta, Y.; Le, T. H.; Sato, T.; Kitagawa, T. *J. Phys. Chem. A* **2002**, *106*, 3436−3444) in combination with DFT calculations. The upshifts of the phenoxyl vibrational frequencies for 8a (C−C stretching), 7a′ (C−O stretching), and 19a, and the Raman-intensity enhancements of 19b, 8b, and 14 modes indicate that UVRR spectra are highly sensitive to imidazole-phenol covalent linkage. Both transient absorption measurements and EPR spectra suggest that the Tyr-His-Cu_B unit has only a minor effect on the electronic structure of the phenoxyl radical form, although our experimental results appear to indicate that the cross-linked Tyr radical exhibits no EPR. The role of the Tyr-His-Cu_B unit in the enzyme is discussed in terms of the obtained spectroscopic parameters of the model complex.

Introduction

Cytochrome *c* oxidase (CcO) is a terminal enzyme of a respiratory chain that catalyzes the $4e^-/4H^+$ reduction of dioxygen to water.[1−4] The reaction is performed at the heme a_3−Cu_B binuclear center without leakage of active oxygen species.[5−7] X-ray crystallographic analysis of CcO has revealed novel characteristics of the Cu_B site, in which one of three histidine residues coordinating to Cu_B is covalently cross-linked to a tyrosine through ϵ-nitrogen of His240 and C6 of Tyr244 (the residue number is based on the bovine enzyme) by a post-translational modification.[8−13] A number of studies on the variants of the superfamily of terminal heme-copper oxidases (HCO) and an engineered heme-copper center in myoglobin have suggested that the covalently linked Tyr-His-Cu_B moiety is indispensable for the enzymatic activity, although its actual role remains to be elucidated.[14−24] Biomimetic approaches to elucidating the reaction mechanism of HCO have been sum-

[†] National Institute of Natural Science.
[‡] Kyushu University.
[§] Tohoku University.

(1) Ferguson-Miller, S.; Babcock, G. T. *Chem. Rev.* **1996**, *96*, 2889−2907.
(2) Yoshikawa, S.; Shinzawa-Itoh, K.; Tsukihara, T. *J. Inorg. Biochem.* **2000**, *82*, 1−7.
(3) Kitagawa, T. *J. Inorg. Biochem.* **2000**, *82*, 9−18.
(4) Ogura, T.; Kitagawa, T. *Biochim. Biophys. Acta* **2004**, *1655*, 290−297.
(5) Kannt, A.; Michel, H. In *Handbook of Metalloproteins*; Messerschmidt, A., Huber, R., Poulos, T., Wieghardt, K., Eds.; Wiley: New York, 2001; Vol. 1, pp 331−347.
(6) Yoshikawa, S.; Shinzawa-Itoh, K.; Yamashita, E.; Tsukihara, T. In *Handbook of Metalloproteins*; Messerschmidt, A., Huber, R., Poulos, T., Wieghardt, K., Eds.; Wiley: New York, 2001; Vol. 1, pp 348−362.
(7) Than, M. E.; Soulimane, T. In *Handbook of Metalloproteins*; Messerschmidt, A., Huber, R., Poulos, T., Wieghardt, K., Eds.; Wiley: New York, 2001; Vol. 1, pp 363−378.
(8) Iwata, S.; Ostermeier, C.; Ludwig, B.; Michel, H. *Nature* **1995**, *376*, 660−669.
(9) Tsukihara, T.; Aoyama, H.; Yamashita, E.; Tomizaki, T.; Yamaguchi, H.; Shinzawa-Itoh, K.; Nakashima, R.; Yaono, R.; Yoshikawa, S. *Science* **1995**, *269*, 1069−1074.
(10) Tsukihara, T.; Aoyama, H.; Yamashita, E.; Tomizaki, T.; Yamaguchi, H.; Shinzawa-Itoh, K.; Nakashima, R.; Yaono, R.; Yoshikawa, S. *Science* **1996**, *272*, 1136−1144.
(11) Ostermeier, C.; Harrenga, A.; Ermler, U.; Michel, H. *Proc. Natl. Acad. Sci. U.S.A.* **1997**, *94*, 10547−10553.
(12) Yoshikawa, S.; Shinzawa-Itoh, K.; Nakashima, R.; Yaono, R.; Yamashita, E.; Inoue, N.; Yao, M.; Fei, M. J.; Libeu, C. P.; Mizushima, T.; Yamaguchi, H.; Tomizaki, T.; Tsukihara, T. *Science* **1998**, *280*, 1723−1729.
(13) Soulimane, T.; Buse, G.; Bourenkov, G. P.; Bartunik, H. D.; Huber, R.; Than, M. E. *EMBO J.* **2000**, *19*, 1766−1776.
(14) Uchida, T.; Mogi, T.; Nakamura, H.; Kitagawa, T. *J. Biol. Chem.* **2004**, *279*, 53613−53620.

10.1021/ja061507y CCC: $33.50

marized in review papers.[25−27] A few model complexes of the heme a_3−Cu_B binuclear center including cross-linked phenol have recently been synthesized and examined for their oxygen reactivity.[28−33] Although the studies of Liu et al.[28,29] implied that phenol acted as a residue delivering a proton to molecular oxygen or fixing a water molecule at the active site, explicit O−O bond cleavage was not achieved, probably due to the lack of an additional single electron for the oxygen reduction. Spectroscopic investigations of the radical state of the model system of the Cu_B site have been conducted only on the Tyr-His cross-linked molecules without the Cu ion,[34−40] and the spectroscopic character of the Tyr-His-Cu_B unit in the highly oxidized state requires clarification. Accordingly, we synthesized the minimal model complex [M-**BIAIP**Br]$^+$; (**BIAIP** = 2-[4-[[bis(1-methyl-*1H*-imidazol-2-ylmethyl)amino]methyl]-*1H*-imidazol-1-yl]-4-methylphenol) as shown in Figure 1a and focused on the role of the imidazole-phenol covalent linkage and thus the electronic interaction between phenol and Cu via the imidazole ring.[28,29,41] Hereafter, we abbreviate the above complex as M-**BIAIP** (where M = Cu^{II}, Zn^{II}).

One of the conundrums remaining in explaining O_2 reduction by CcO is the electronic structure of the so-called P intermediate.[3,4,42] Time-resolved Raman spectroscopy has established that O−O bond cleavage is completed on the stage of the P intermediate,[43] but the location of an oxidative equivalent additional to the ferryl-oxo heme is a matter of debate. Plausible candidates for it include the porphyrin ring, tryptophan or tyrosine residue, and Cu_B.[44−46]

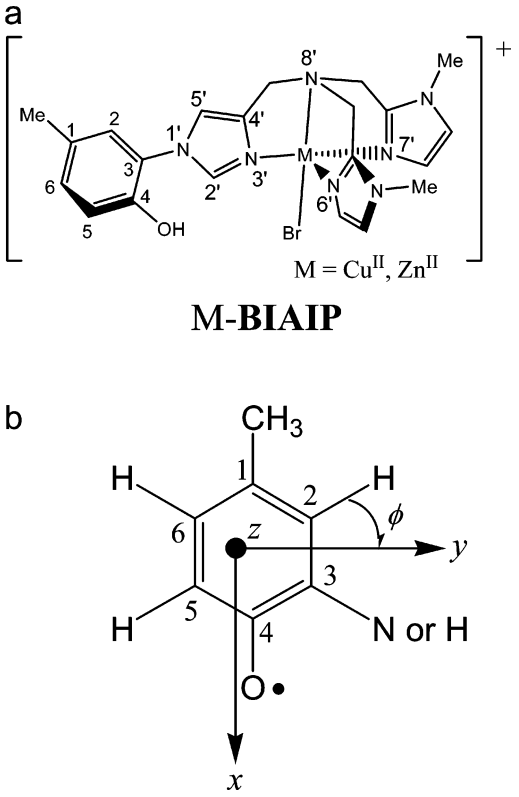

Figure 1. (a) Schematic of the M-**BIAIP** (M = Cu^{II}, Zn^{II}) complex, and (b) principal axes of the ***g*** tensor in phenoxyl radicals. Angle ϕ represents an in-plane rotation of the principal axes of the hyperfine tensors relative to the ***g***-axes system.

In this study, we performed steady-state and transient absorption measurements, UV resonance Raman (UVRR) spectroscopy, X-band continuous-wave electron paramagnetic resonance (EPR) spectroscopy, and density functional theory (DFT) calculations to **BIAIP**s to elucidate a spectroscopic basis for the putative Tyr244 radical and to explore the physicochemical properties of the Tyr-His-Cu_B moiety. Significant reductions of the pK_a values of phenolic hydroxide have been reported for Tyr-His models, which is probably attributable to proton delivery to the heme a_3−Cu_B binuclear center.[26,34,36,38,47] Thus, the pH dependency of absorption spectra was also measured to clarify the acidity of the phenolic OH group for the parent molecule. To investigate the radical states, we combined the above spectroscopy techniques with UV-light irradiation, which is an excellent method for generating radicals with few side reactions.[34,48−54] Irradiation with high-intensity UV laser light

(15) Pinakoulaki, E.; Pfitzner, U.; Ludwig, B.; Varotsis, C. *J. Biol. Chem.* **2002**, *277*, 13563−13568.
(16) Mogi, T.; Minagawa, J.; Hirano, T.; Sato-Watanabe, M.; Tsubaki, M.; Uno, T.; Hori, H.; Nakamura, H.; Nishimura, Y.; Anraku, Y. *Biochemistry* **1998**, *37*, 1632−1639.
(17) Das, T. K.; Pecoraro, C.; Tomson, F. L.; Gennis, R. B.; Rousseau, D. L. *Biochemistry* **1998**, *37*, 14471−14476.
(18) Mogi, T.; Hirano, T.; Nakamura, H.; Anraku, Y.; Orii, Y. *FEBS Lett.* **1995**, *370*, 259−263.
(19) Tsubaki, M.; Mogi, T.; Hori, H.; Hirota, S.; Ogura, T.; Kitagawa, T.; Anraku, Y. *J. Biol. Chem.* **1994**, *269*, 30861−30868.
(20) Thomas, J. W.; Calhoun, M. W.; Lemieux, L. J.; Puustinen, A.; Wikström, M.; Alben, J. O.; Gennis, R. B. *Biochemistry* **1994**, *33*, 13013−13021.
(21) Saiki, K.; Mogi, T.; Hori, H.; Tsubaki, M.; Anraku, Y. *J. Biol. Chem.* **1993**, *268*, 26927−26934.
(22) Calhoun, M. W.; Hill, J. J.; Lemieux, L. J.; Ingledew, W. J.; Alben, J. O.; Gennis, R. B. *Biochemistry* **1993**, *32*, 11524−11529.
(23) Lemon, D. D.; Calhoun, M. W.; Gennis, R. B.; Woodruff, W. H. *Biochemistry* **1993**, *32*, 11953−11956.
(24) Sigman, J. A.; Kim, H. K.; Zhao, X.; Carey, J. R.; Lu, Y. *Proc. Natl. Acad. Sci. U.S.A.* **2003**, *100*, 3629−3634.
(25) Collman, J. P.; Boulatov, R.; Sunderland, C. J.; Fu, L. *Chem. Rev.* **2004**, *104*, 561−588.
(26) Kim, E.; Chufán, E. E.; Kamaraj, K.; Karlin, K. D. *Chem. Rev.* **2004**, *104*, 1077−1133.
(27) Boulatov, R.; Collman, J. P.; Shiryaeva, I. M.; Sunderland, C. J. *J. Am. Chem. Soc.* **2002**, *124*, 11923−11935.
(28) Liu, J. G.; Naruta, Y.; Tani, F. *Angew. Chem., Int. Ed.* **2005**, *44*, 1836−1840.
(29) Liu, J. G.; Naruta, Y.; Tani, F.; Chishiro, T.; Tachi, Y. *Chem. Commun.* **2004**, 120−121.
(30) Kim, E.; Kamaraj, K.; Galliker, B.; Rubie, N. D.; Moënne-Loccoz, P.; Kaderli, S.; Zuberbuhler, A. D.; Karlin, K. D. *Inorg. Chem.* **2005**, *44*, 1238−1247.
(31) Kamaraj, K.; Kim, E.; Galliker, B.; Zakharov, L. N.; Rheingold, A. L.; Zuberbühler, A. D.; Karlin, K. D. *J. Am. Chem. Soc.* **2003**, *125*, 6028−6029.
(32) Collman, J. P.; Decreau, R. A.; Cosranzo, S. *Org. Lett.* **2004**, *6*, 1033−1036.
(33) Collman, J. P.; Decreau, R. A.; Zhang, C. *J. Org. Chem.* **2004**, *69*, 3546−3549.
(34) Aki, M.; Ogura, T.; Naruta, Y.; Le, T. H.; Kitagawa, T. *J. Phys. Chem. A* **2002**, *106*, 3436−3444.
(35) Kim, S. H.; Aznar, C.; Brynda, M.; Silks, L. A.; Michalczyk, R.; Unkefer, C. J.; Woodruff, W. H.; Britt, R. D. *J. Am. Chem. Soc.* **2004**, *126*, 2328−2338.
(36) Cappuccio, J. A.; Ayala, I.; Elliott, G. I.; Szundi, I.; Lewis, J.; Konopelski, J. P.; Barry, B. A.; Einarsdóttir, Ó. *J. Am. Chem. Soc.* **2002**, *124*, 1750−1760.
(37) Barry, B. A.; Einarsdóttir, Ó. *J. Phys. Chem. B* **2005**, *109*, 6972−6981.
(38) McCauley, K. M.; Vrtis, J. M.; Dupont, J.; van der Donk, W. A. *J. Am. Chem. Soc.* **2000**, *122*, 2403−2404.
(39) Elliott, G. I.; Konopelski, J. P. *Org. Lett.* **2000**, *2*, 3050−3057.
(40) Pratt, D. A.; Pesavento, R. P.; van der Donk, W. A. *Org. Lett.* **2005**, *7*, 2735−2738.
(41) Nagano, Y.; Liu, J.-G.; Naruta, Y.; Kitagawa, T. *J. Mol. Struct.* **2005**, *735−736*, 279−291.
(42) Einarsdóttir, Ó.; Szundi, I.; Van Eps, N.; Sucheta, A. *J. Inorg. Biochem.* **2002,** *91*, 87−93.
(43) Ogura, T.; Hirota, S.; Proshlyakov, D. A.; Shinzawa-Itoh, K.; Yoshikawa, S.; Kitagawa, T. *J. Am. Chem. Soc.* **1996**, *118*, 5443−5449.
(44) Rich, P. R.; Rigby, S. E.; Heathcote, P. *Biochim. Biophys. Acta* **2002**, *1554*, 137−146.
(45) Rigby, S. E.; Jünemann, S.; Rich, P. R.; Heathcote, P. *Biochemistry* **2000**, *39*, 5921−5928.
(46) MacMillan, F.; Kannt, A.; Behr, J.; Prisner, T.; Michel, H. *Biochemistry* **1999**, *38*, 9179−9184.
(47) Collman, J. P.; Wang, Z.; Zhong, M.; Zeng, L. *J. Chem. Soc., Perkin Trans. 1* **2000**, 1217−1221.

causes photoelectron emission, leading to generation of the phenoxyl radical. Together the experimental results reveal that both the imidazole-phenol cross-linkage and Cu^{II} coordination cause only a minor modification to the electronic structure of the ground state of the parent molecule as well as its radical. The role of the Tyr-His-Cu_B moiety in the enzyme is also discussed. The principal axis system of the ***g*** tensor for phenoxyl radicals and the Euler angle for transforming the system from this tensor to a proton hyperfine frame are defined in Figure 1b.

Experimental Section

Detailed descriptions of syntheses of **BIAIP** models[41] and our UVRR instruments are available elsewhere.[28,29,34,55] Most of the sample solutions were adjusted to 2.5 mM at pH 13 except where stated otherwise; under these conditions, phenolic OH protons are dissociated, as confirmed by the absorption spectra.[41]

pH Dependency of Absorption Spectra. UV absorption spectra were measured with a Hitachi U-3310 spectrophotometer. The final concentrations of Cu^{II}-**BIAIP** and *p*-cresol were adjusted to 25 and 100 μM, respectively, at different pH values using the following solvents: HCl for pH 2∼5.4, 0.1 M acetate buffer for pH 3.4∼5.6, 0.1 M phosphate buffer for pH 6.4∼7.7, 0.0125 M borate buffer for pH 8.0∼8.7, 0.05 M borate buffer for pH 8.1∼10.2, 0.025 M phosphate buffer for pH 10.9∼11.7, and 0.1 M NaOH for pH 13. The solution pH was measured with a Beckman 720 pH meter.

UV Resonance Raman Measurements. Raman spectra were observed with intense 10-ns pulsed laser light (1.3 mJ/pulse, 10 Hz) at 240 nm; complete experimental details are available elsewhere.[34,55] The spectra of phenoxyl radicals were obtained from the digital subtraction of the contribution of the phenolate, which was measured with the same sample solution under a low laser intensity (25 μJ/pulse, 100 Hz),[41] from the spectra observed with a high laser intensity.[34] For most of the sample solutions, 600 mM Na_2SO_4 was added as an internal intensity standard, and spectra are presented or subtracted on the basis of the 981-cm^{-1} band of SO_4^{2-}.

Transient Absorption Measurements. Oxygen was removed in advance of and during measurements by bubbling N_2 into sample solutions. A detector controller (Princeton Instruments, ST121) was synchronized with the fourth harmonic of a Nd:YAG laser (Spectra-Physics INDI-20, 266 nm, 2.4 mJ/pulse, 20 Hz) using pulse generators (Princeton Instruments FG-100; Stanford DG535; EG&G 965A). Radiation from the laser and Xe lamp was collected into an 1-cm-long quartz cuvette containing the sample solution at room temperature. The transient absorption spectra and time profiles of signals were detected by an intensified photodiode array (Princeton Instruments SMA IRY-700) and a photomultiplier (Hamamatsu Photonics 285), respectively, after the light from the Xe lamp was dispersed by a monochromator (McPHERSON 2035). The output from the photomultiplier was fed to a low-noise preamplifier (NF SA-230F5) and then to a digital oscilloscope (SONY Tektronix TDS520D). The time response of the instrumental setup was ca. 40 ns. The performance of the system was verified by measuring the spectrum and the time profile of the 2,4,6-tri-*tert*-butylphenoxyl radical in methanol and comparing this with the spectrum obtained with the chemical oxidation by $K_4[Fe^{II}(CN)_6]$ (see Figure S1, Supporting Information).

EPR Measurements. The phenoxyl radicals were generated by irradiating with the UV light (2.5 W/cm^2 at a sample position) from a 500 W mercury-arc lamp (Ushio USH 500H) for a few minutes. Conventional X-band CW-EPR spectra were obtained using a Bruker ESP-380E or Bruker E500 with 100-kHz field modulation. A helium flow cryostat (Oxford ESR900) was used to perform measurements at low temperatures. The spectra were simulated with commercially available software (Bruker).

Computational Methods

DFT calculations were performed with the Gaussian 03 program package (Revision B.05) installed on SGI Origin2000, SGI2800, Origin3800, and NEC TX7 computers operated by the Research Center for Computational Science at Okazaki.[56] A 6-31G* set of Gaussian functions was adopted as the basis function. Becke's three-parameter hybrid method using the correlation functional developed by Lee, Yang, and Parr (B3LYP) was employed.[57]

Results

pH Dependency of Absorption Spectra. Proton delivery from a nearby residue is essential to derive a water molecule from the heme bound dioxygen, and Tyr244 is one of the plausible candidates of a proton donor. To determine the effect of the imidazole-phenol cross-linkage and the Cu^{II} coordination on the acidity of the phenolic OH group, we measured the pH dependency of the absorption spectra for Cu^{II}-**BIAIP** using *p*-cresol as a reference. Factor analyses were used to determine their pK_a values,[58] because the data set of Cu^{II}-**BIAIP** spectra shows a somewhat complicated pH dependency, probably due to the medium.[59] From photometric titration of *p*-cresol in the range of pH = 1.6−12.8 (Figure S2), the pK_a value of *p*-cresol was determined to be 10.2, which is in good agreement with the reported value.[34,36−38,41]

Although an excess amount of KCl in solutions is preferable to maintain a constant ionic strength, the experiments were first carried out without KCl due to the relatively low solubility of Cu^{II}-**BIAIP** (the only effect of KCl is to shift the pK_a value to a slightly lower value). We later found that Cu^{II}-**BIAIP** is sufficiently soluble even after the addition of 0.3 M KCl. Similar to Figure S2 for *p*-cresol, Figure 2a shows the pH dependency of Cu^{II}-**BIAIP** absorption spectra for pH values from 2.0 to 12.9. Application of factor analysis extracted the absorption spectra of three principal components (Figure 2b) and yielded two pK_a values: 4.9 and 10.2. The isosbestic point at 295.6 nm was clearly revealed by reconstruction of the data set (Figure 2a′). From the fraction indicated in Figure 2c, three dominant components in the acidic, neutral, and basic pH regions could be definitively assigned to the fully protonated form, where both cross-linked imidazole and phenolic OH are fully protonated (dotted-dashed line), OH-protonated (solid line), and OH-deprotonated (dotted line), respectively (Figure 2b). A redshift of the L_b band from 288.4 to 307.6 nm was observed as the pH increased from neutral to basic values. When the pH decreased from a neutral value, the shoulder around 330 nm became weaker, and the L_b band exhibited a slight redshift to 290.0 nm with a concomitant decrease in intensity. These behaviors and the spectral characteristics are similar to those of Tyr-His models

(48) Bussantri, A.; van Willigen, H. *J. Phys. Chem. A* **2001**, *105*, 4669−4675.
(49) Bussantri, A.; van Willigen, H. *J. Phys. Chem. A* **2002**, *106*, 1524−1532.
(50) Grabner, G.; Köhler, G.; Zechner, J.; Getoff, N. *Photochem. Photobiol.* **1977**, *26*, 449−458.
(51) Grabner, G.; Köhler, G.; Zechner, J.; Getoff, N. *J. Phys. Chem.* **1980**, *84*, 3000−3004.
(52) Bent, D. V.; Hayon, E. *J. Am. Chem. Soc.* **1975**, *97*, 2599−2606.
(53) Mialocq, J.-C.; Sutton, J.; Goujon, P. *J. Chem. Phys.* **1980**, *72*, 6338−6345.
(54) Hulsebosch, R. J.; van den Brink, J. S.; Nieuwenhuis, S. A. M.; Gast, P.; Raap, J.; Lugtenburg, J.; Hoff, A. J. *J. Am. Chem. Soc.* **1997**, *119*, 8685−8694.
(55) Kaminaka, S.; Kitagawa, T. *Appl. Spectrosc.* **1992**, *46*, 1804−1808.
(56) Frisch, M. J. et al. *Gaussian 03*, revision B.05; Gaussian, Inc.: Pittsburgh, PA, 2003.
(57) Becke, A. D. *J. Chem. Phys.* **1993**, *98*, 5648−5652.
(58) Malinowski, E. R. *Factor Analysis in Chemistry*, 3rd ed.; John Wiley and Sons: New York, 2002.
(59) Edward, J. T.; Wong, S. C. *J. Am. Chem. Soc.* **1977**, *99*, 4229−4232.

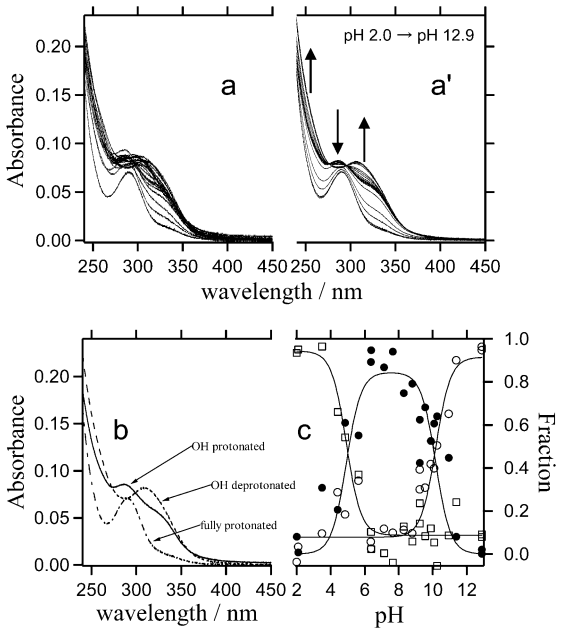

Figure 2. (a) pH-dependent UV−visible absorption spectra of a 25-μM aqueous solution of Cu^{II}-**BIAIP** for pH values from 2.0 to 12.9, and (a′) the data reconstructed by factor analysis. The extracted components and the fractions corresponding to fully protonated (dotted-dashed, □), phenolic OH-protonated (solid line, ●), and deprotonated (dashed line, ○) forms are shown in (b) and (c), respectively. (c) The theoretical curves with pK_a values of 4.9 and 10.2 are also displayed as solid lines.

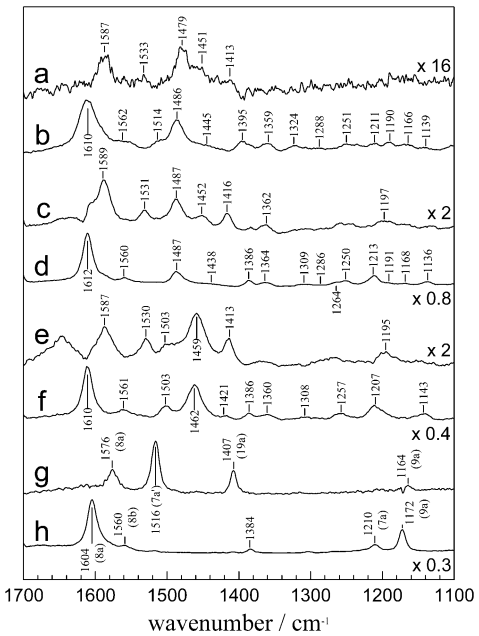

Figure 3. UVRR spectra of radical forms (a, c, e, g) and parent phenolate forms (b, d, f, h) excited at 240 nm at pH 13 (100 mM NaOH aqueous solution): Cu^{II}-**BIAIP** (a, b), Zn^{II}-**BIAIP** (c, d), metal-free **BIAIP** (e, f), and *p*-cresol (g, h). The spectra of the radical forms are the differences between the high- and low-intensity spectra, and their intensities are estimated using the 981-cm^{-1} band of SO_4^{2-} as an internal intensity standard (see text). Although the true intensities of the parent molecules are 70, 40, 40, and 40% of their low-intensity spectra for Cu^{II}-, Zn^{II}-, metal-free **BIAIP**, and *p*-cresol, respectively, they are each normalized to their maximum intensity in this figure.

reported by Aki et al.[34] and Einarsdóttir and co-workers.[36,37] Our observations suggest that the Cu^{II}-N3′ bond is cleaved at around pH 4.9.

The absorption in the pH range from 6.9 to 12.9 was also measured for Cu^{II}-**BIAIP** solution with 0.3 M KCl (see Figure S3, Supporting Information). Application of the same analysis as described above yielded a pK_a value of 9.8, which indicates that phenolic OH is acidic. The difference between the pK_a values obtained for Cu^{II}-**BIAIP** (9.8) and *p*-cresol (10.2) under the 0.3-M-KCl condition is subtle despite the introduction of the imidazole-phenol cross-linkage and Cu^{II} coordination. Moreover, this contrasts with previous reports that the pK_a of phenolic OH for Tyr-His models was significantly lower than that of *p*-cresol, ranging from 6.58 to 9.2.[34,36−38,47] On the other hand, the pK_a of normal imidazole (6.65 or 7.10)[34,60] lowers to 4.05∼6.12 in the presence of cross-linking with phenol.[34,36−38,47] A relatively large dihedral angle between the phenol and imidazole planes would reduce the π conjugation between the two rings, hence resulting in pK_a values similar to those of the nonsubstituted phenols. Other possible components arising from the protonation of N8′, whose pK_a ranges between 9.80 (trimethylamine) and 10.75 (triethylamine),[61] are too difficult to recognize in our analysis. This implies the presence of negligible interaction between Cu^{II} and N8′, which is expected from the longer bond distance calculated by DFT as described below (also see Table S1, Supporting Information).

UV Resonance Raman Spectroscopy. It is desirable to find a candidate Raman band assignable to tyrosine radical in the UVRR spectra of the P intermediate of the enzyme. Figure 3 shows UVRR spectra of the radical forms (Figure 3a,c,e,g) and the corresponding parent molecules (Figure 3b,d,f,h) excited at 240 nm at pH 13, at which phenolic OH protons are dissociated (as confirmed by the absorption spectra).[41] The spectra of parent molecules are scaled by the use of the 981-cm^{-1} band of SO_4^{2-} (as an intensity standard), and both the band assignments and the scattering cross sections for the observed bands are reported elsewhere.[41] The spectra of the **BIAIP** radicals are expanded in the ordinate in relation to those of *p*-cresol. When the same experimental conditions were used, the relative intensities of parent molecules in the high-laser-intensity spectra were ca. 70, 40, 40, and 40% of those observed with the low-laser-intensity condition for the phenolate forms of Cu^{II}-**BIAIP**, Zn^{II}-**BIAIP**, metal-free **BIAIP**, and *p*-cresol, respectively. The intensity reduction of the parent molecules under a higher laser intensity is due to more effective photoconversion to the radical forms, although the effectiveness varies with the species. Figure 3g shows three prominent Raman bands at 1576, 1516, and 1407 cm^{-1} that are assignable to 8a (C−C stretching), 7a′ (C−O stretching), and 19a of phenol, respectively, which are characteristic of the phenoxyl radical.[34,62−64] The spectral patterns of the radical forms of **BIAIP**s are almost the same as that of 2-(1-imidazoyl)-4-methylphenoxyl (Im-PhO•) reported previously.[34] Therefore, the band assignments of Im-PhO• may be directly applicable to **BIAIP**s. The Im-PhO• isotope shifts reported by Aki et al.[34] combined with DFT calculations enable precise band assignments, as described in the section entitled "DFT Calcula-

(60) Franzen, S.; Boxer, S. G.; Dyer, R. B.; Woodruff, W. H. *J. Phys. Chem. B* **2000**, *104*, 10359−10367.
(61) *CRC Handbook of Chemistry and Physics*, 86th ed.; CRC Press: Boca Raton, FL, 2005.
(62) Johnson, C. R.; Ludwig, M.; Asher, S. A. *J. Am. Chem. Soc.* **1986**, *108*, 905−912.
(63) Mukherjee, A.; McGlashen, M. L.; Spiro, T. G. *J. Phys. Chem.* **1995**, *99*, 4912−4917.
(64) McGlashen, M. L.; Eads, D. D.; Spiro, T. G.; Whittaker, J. W. *J. Phys. Chem.* **1995**, *99*, 4918−4922.

Table 1. Selected Vibrational Frequencies (cm^{-1}) and Assignments for Phenoxyl Radicals

Cu^{II}-**BIAIP**		Zn^{II}-**BIAIP**		**BIAIP**	Im-PhO•		*p*-cresol		
obs	calc	obs	calc	obs	obs[b]	calc	obs	calc	assignments[a]
1587	1629	1589	1628	1587	1587	1635	1576	1619	8a (C−C str)
1533	1550	1531	1550	1530	1530	1553	1516	1515	7a′ (C−O str)
1479	1497	1487	1498		1488	1500		1459	19b + C3−N1′ str
1451	1471	1451	1472		1449	1484		1540	8b
1413	1455	1416	1455	1413	1409	1455	1407	1447	19a

[a] Wilson-mode descriptions for the phenols; see refs 63, 98, and 104 for further details. [b] Reference 34.

tions". The observed and calculated Raman frequencies and band assignments are summarized in Tables 1 and S6 (see Supporting Information).

Similar sets of Raman bands were observed for the radical forms of Cu^{II}-**BIAIP** (Figure 3a; 1587, 1533, 1413 cm^{-1}, 1/16 times the intensity relative to *p*-cresol, see caption), Zn^{II}-**BIAIP** (Figure 3c; 1589, 1531, 1416 cm^{-1}, 1/2 times the intensity), and metal-free **BIAIP** (Figure 3e; 1587, 1530, 1413 cm^{-1}, 1/2 times the intensity). This indicates that metal coordination hardly affects the vibrational frequencies of phenoxyl-radical modes, although the Raman intensity of the radical form is especially weak for Cu^{II}-**BIAIP**. This is probably due to the change in the oxidation potential, the contribution of a rapid intramolecular electron transfer between phenolate/Cu^{I} and phenoxyl radical/Cu^{II} states, or decreased stability of the radical state. We attempted to obtain an RR spectrum of a chemically prepared radical state of Cu^{I}-**BIAIP** in order to clarify these points, but spectral isolation was not successful because of the contamination of Cu^{II}-**BIAIP**. These three Raman bands can be reliably assigned to the phenoxyl 8a (C−C stretching), 7a′ (C−O stretching), and 19a vibrations. All three modes are shifted toward higher frequencies relative to those of *p*-cresol, which is due to the imidazole-phenol cross-linkage. As seen in the absorption spectra (Figure 2a−d in ref 41), the phenolate L_a bands around 240 nm become less noticeable in the order of *p*-cresolate > Zn^{II}-**BIAIP**, metal-free **BIAIP** (phenolic OH-deprotonated, O^- form) > Cu^{II}-**BIAIP** (O^- form). The Raman excitation profile also exhibits the same trend.[41] Other absorption bands appear to be overlapped with the L_a absorption for Cu^{II}-**BIAIP**, which makes selective excitation of the phenol moiety difficult. This is the reason only Cu^{II}-**BIAIP** exhibits such a weak Raman intensity. For Zn^{II}-**BIAIP** and *p*-cresol, the same radical spectra were also observed even at pH 6.4, although the Raman intensities are 1/3 and 1/6 times, respectively, that of *p*-cresol at pH 13.[38,62,65−67]

The bands at 1479 cm^{-1} for Cu^{II}-**BIAIP** (Figure 3a), at 1487 cm^{-1} for Zn^{II}-**BIAIP** (Figure 3c), and at 1503 and 1459 cm^{-1} for metal-free **BIAIP** (Figure 3e) are correspondingly observed in the spectra of parent molecules with pronounced intensities (Figure 3b,d,f). These Raman bands are assigned to modes of imidazoles not linked to phenol, and their intensities are enhanced by the preresonance to the lowest $\pi\pi^*$ transition of imidazole.[41] The two imidazole groups not linked to phenol in each complex are less likely to be influenced by the formation of the phenoxyl radical. Thus, there is a possibility that the laser-intensity dependency of the Raman enhancement for phenolate bands differs from that of the parent non-cross-linked imidazole. Different laser-intensity dependencies would cause an incomplete subtraction of the signals of the parent molecules from the high-laser-intensity spectra. To distinguish whether the Raman bands arise from the parent or radical species, laser-intensity dependencies of UVRR spectra were measured (Figures S4 and S5, Supporting Information). On the basis of our factor analyses (Figures S6 and S7, Supporting Information), we confirmed that the Raman bands (1576, 1516, 1407, 1276, 1228, and 1164 cm^{-1} for *p*-cresol, and 1587, 1531, 1487, 1451, 1416, 1366, 1324, 1283, 1261, 1192, and 1174 cm^{-1} for Zn^{II}-**BIAIP**) were ascribed to those of radical form.

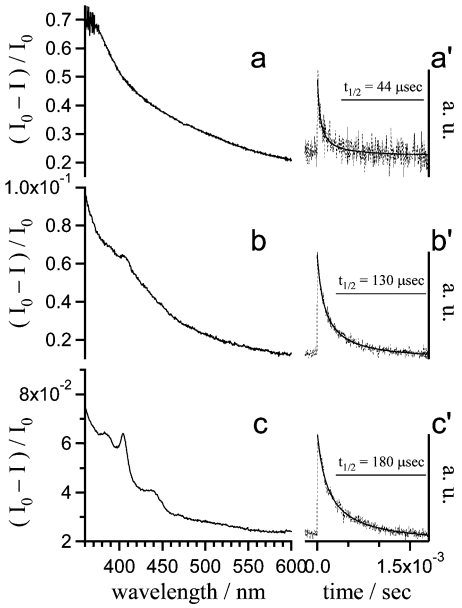

Figure 4. (a, b, c) Transient absorption spectra and (a′, b′, c′) time profiles monitored at 400 nm for (a, a′) Cu^{II}-**BIAIP**, (b, b′) Zn^{II}-**BIAIP**, and (c, c′) *p*-cresol following irradiation at 266 nm.

Transient Absorption. Figure 4 shows the transient absorption spectra of Cu^{II}-**BIAIP** (a), Zn^{II}-**BIAIP** (b), and *p*-cresol (c) observed at a few microseconds after laser excitation at 266 nm. The time profiles monitored at around 400 nm are also indicated (Figures 4a′,b′, and c′). I_0 and I denote the intensities of the radiation from a Xe lamp that passed through the sample without and with the 266-nm laser pulse, respectively. The absorbance of transient species can be approximated as $(I_0 - I)/I_0$ when the transmittance is close to 100%. The typical doublet bands ascribable to the phenoxyl radical produced upon the photolysis of *p*-cresol are evident at 404 and 386 nm (Figure 4c).[50,68−76] A similar doublet is also evident for Zn^{II}-**BIAIP** at 407 and 389 nm (Figure 4b), also indicating the formation of the phenoxyl radical.[77] On the other hand, Figure 4a suggests that Cu^{II}-**BIAIP** is very photolabile with a rather broad spectrum.

(65) Diner, B. A. *Biochim. Biophys. Acta* **2001**, *1503*, 147−163.
(66) Steenken, S.; Neta, P. *Transient phenoxyl radicals: Formaton and properties in aqueous solutions*; Wiley: West Sussex, England, 2003; Part 2, p 1133.

However, a decay of the absorbance with a half-life of 44 μs was observed around 400 nm. Compared with the half-lives of 130 and 180 μs for Zn^{II}-**BIAIP** (Figure 4b′) and *p*-cresol (Figure 4c′), respectively,[78] the lower value for Cu^{II}-**BIAIP** (Figure 4a′) is probably due to a reaction such as dimerization from their radical states. Thus, we concluded that the phenoxyl radical was created. The obtained decay curves were analyzed using the following equation for a second-order reaction:

$$\frac{I_0 - I}{I_0} = \frac{\epsilon[\mathrm{A}]_0}{1 + kt[\mathrm{A}]_0} \quad (1)$$

where ϵ, $[A]_0$, k, and t are the molar extinction coefficient, the initial concentration of reactant A, the second-order rate constant, and time, respectively. ϵ was fixed at the reported value of 3550 M^{-1} cm^{-1} for all analyses.[73−75] The estimated second-order rate constants were 2×10^8, 2×10^6, and 6×10^6 M^{-1} s^{-1}, for Cu^{II}-**BIAIP**, Zn^{II}-**BIAIP**, and *p*-cresol, respectively. The larger value for Cu^{II}-**BIAIP** probably reflects the characteristics of Cu^{II} coordination to the phenoxyl-imidazole unit. The band positions of phenoxyl radicals and the rate constant suggest that the effects of the imidazole-phenol covalent as well as metal coordination to the cross-linked imidazole on the electronic structure of the phenoxyl radical are minor.

EPR. To confirm the presence of phenoxyl radicals and to explore their electronic structures, X-band continuous-wave EPR measurements were performed in combination with UV-light irradiation. As shown in Figure 5, the spectra of phenoxyl radicals—whose lifetime lengthened at low temperatures—were successfully observed for Zn^{II}-**BIAIP** (Figure 5b) and *p*-cresol (Figure 5c) and were in good agreement with those reported previously.[35,38,79] An identical spectrum was also obtained for *p*-cresol even at pH 6.4. This observation is consistent with the previous reports as well as our UVRR results described above indicating that the same radical species was formed due to the high acidity of a protonated radical.[38,54,62,65,66] On the other hand, Figure 5a indicates that the spectrum of Cu^{II}-**BIAIP** was completely different from those of the other compounds. No difference was detected in the signal intensity or spectral pattern before and after UV-light irradiation (even with continuous irradiation during measurements). However, the detected signals spread out in a wide field region and the intensity was much

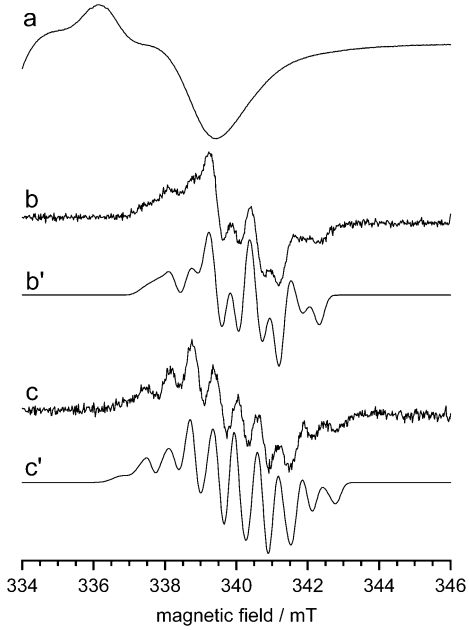

Figure 5. Observed and simulated EPR spectra of the radical forms of (b, b′) Zn^{II}-**BIAIP** and (c, c′) *p*-cresol. (a) For Cu^{II}-**BIAIP**, only the EPR signal from the parent molecule is observed. The spectra were observed at 77 K.

stronger (ca. 1500 times) compared to the radical forms of Zn^{II}-**BIAIP** and *p*-cresol. The signal intensity and uniaxial spectral pattern with large hyperfine splittings due to the Cu^{II} ion having $I = 3/2$ indicate that the observed spectrum should be assigned to the parent molecule. This was confirmed by a spectrum simulation employing the $S = {}^1/_2$ state with the parameters $g_{||} = 2.27$, $g_\perp = 2.05$, $A_{||} = 19$ mT, and $A_\perp = 3.6$ mT (Figure S8, Supporting Information), which are typical values for Cu^{II} complexes.[31,80−86] On the basis of our DFT calculation, the ground and excited states of the Cu^{II}-**BIAIP** radical form correspond to $S = 1$ and $S = 0$, respectively; their frequency separation was estimated to be a few cm^{-1}. Therefore, it is expected that the EPR spectrum of the Cu^{II}-**BIAIP** radical form reflects a triplet state, which may exhibit the mean values of the individual magnetic parameters for phenoxyl and Cu^{II}. To examine the possibility of the ground or the excited triplet states of the Cu^{II}-**BIAIP** radical form being present, we measured the EPR spectrum from 4 to 90 K. However, no signals attributable to the radical form were detected in this temperature range. Unfortunately, since a phenoxyl radical appears to be rapidly quenched above ca. 90 K for the radical forms of Zn^{II}-**BIAIP** and *p*-cresol, we were unable to perform the analogous measurements at higher temperatures for the Cu^{II}-**BIAIP** radical form. The failure to detect any signals is probably attributable to the low signal intensity of the radical form. The low density

(67) In contrast to the measurement at pH 6.4, the Raman signals due to a photoproduct were in some cases observed at 1589 and 1452 cm^{-1} for Zn^{II}-**BIAIP** at pH 13, which depends on the focal position of the excitation laser beam. The signals of the radical and the photoproduct are accidentally overlapped at 1589 cm^{-1}. No photoproduct was detected by ESI-MS.
(68) Tripathi, G. N. R.; Schuler, R. H. *J. Chem. Phys.* **1984**, *81*, 113−121.
(69) Itoh, S.; Takayama, S.; Arakawa, R.; Furuta, A.; Komatsu, M.; Ishida, A.; Takamuku, S.; Fukuzumi, S. *Inorg. Chem.* **1997**, *36*, 1407−1416.
(70) Tripathi, G. N. R. In *Advances in Spectroscopy*; Clark, R. J. H., Hester, R. E., Ed.; Wiley: New York, 1989; Vol. 18, pp 157−218.
(71) Schuler, R. H.; Neta, P.; Zemel, H.; Fessenden, R. W. *J. Am. Chem. Soc.* **1976**, *98*, 3825−3831.
(72) Alfassi, Z. B.; Shoute, L. C. T. *Int. J. Chem. Kinet.* **1993**, *25*, 79−90.
(73) Bansal, K.; Fessenden, R. W. *Radiat. Res.* **1976**, *67*, 1−8.
(74) Roder, M.; Wojnárovits, L.; Földiák, G.; Emmi, S. S.; Beggiato, G.; D′Angelantonio, M. *Radiat. Phys. Chem.* **1999**, *54*, 475−479.
(75) Alfassi, Z. B.; Schuler, R. H. *J. Phys. Chem.* **1985**, *89*, 3359−3363.
(76) The origin of the band around 440 nm with relatively short lifetime (∼1 μs) is not clear at this moment. That band disappears with continuous laser irradiation. It could arise from some impurities or triplet species.
(77) Wrong species were likely to be observed for the Tyr-Im model in ref 36 judging from the band position and the lifetimes.
(78) Although the single-exponential function never provides satisfactory fit, the best values with that function corresponding to the lifetime are 160, 340, and 310 μs for Cu^{II}-**BIAIP**, Zn^{II}-**BIAIP**, and *p*-cresol, respectively.
(79) The qualities of the CW-EPR spectral simulations for phenoxyl radicals are not good in ref 35.
(80) Whittaker, M. M.; Duncan, W. R.; Whittaker, J. W. *Inorg. Chem.* **1996**, *35*, 382−386.
(81) Zurita, D.; Gautier-Luneau, I.; Ménage, S.; Pierre, J.-L.; Saint-Aman, E. *J. Biol. Inorg. Chem.* **1997**, *2*, 46−55.
(82) Wang, Y.; DuBois, J. L.; Hedman, B.; Hodgson, K. O.; Stack, T. D. *Science* **1998**, *279*, 537−540.
(83) Halfen, J. A.; Jazdzewski, B. A.; Mahapatra, S.; Berreau, L. M.; Wilkinson, E. C.; Que, L., Jr.; Tolman, W. B. *J. Am. Chem. Soc.* **1997**, *119*, 8217−8227.
(84) Chaudhuri, P.; Hess, M.; Müller, J.; Hildenbrand, K.; Bill, E.; Weyhermüller, T.; Wieghardt, K. *J. Am. Chem. Soc.* **1999**, *121*, 9599−9610.
(85) Sokolowski, A.; Leutbecher, H.; Weyhermüller, T.; Schnepf, R.; Bothe, E.; Bill, E.; Hildebrandt, P.; Wieghardt, K. *J. Biol. Inorg. Chem.* **1997**, *2*, 444−453.
(86) Taki, M.; Kumei, H.; Nagatomo, S.; Kitagawa, T.; Itoh, S.; Fukuzumi, S. *Inorg. Chim. Acta* **2000**, *300−302*, 622−632.

Table 2. Proton Hyperfine Splittings, Euler Angles (ϕ), and g Principal Values for Phenoxyl Radicals

hfi	A_{xx}/mT	A_{yy}/mT	A_{zz}/mT	A_{iso}/mT	ϕ/deg
		Zn^{II}-**BIAIP**			
C_1-H_{Me}				1.12	
$C_{2,6}-H$	0.17	0.27	0.04	0.16	±30
C_5-H	−0.75	−0.22	−0.55	−0.51	−23
		p-cresol[a]			
C_1-H_{Me}				1.22	
$C_{2,6}-H$	0.17	0.27	0.16	0.14	±30
$C_{3,5}-H$	−0.96	−0.28	−0.70	−0.61	±23
	$g_{xx} = 2.0068$[b], $g_{yy} = 2.0043$[b], $g_{zz} = 2.0023$[b]				

[a] Line width for simulation: $B_x = 0.40$ mT, $B_y = B_z = 0.25$ mT. [b] Reference 54.

of the long-lived radical form (created by irradiation) and the efficient spin relaxation due to the magnetic interaction between paramagnetic centers[82−88] would presumably result in a weak and broad spectrum that appears beneath the strong spectrum of the parent molecule, which would make its detection difficult.

The EPR spectra of phenoxyl radicals mainly consist of the hyperfine splittings of methyl protons and ortho protons. The slightly narrower distribution of the EPR signal exhibited by Zn^{II}-**BIAIP** relative to *p*-cresol is partly due to the lack of one ortho proton in the imidazole-phenol cross-linkage. We employed the ***g*** values and hyperfine splittings of ring protons reported by Hulsebosch et al.[54] and Hoganson and Babcock[89] for the simulation of the *p*-cresol radical (Figure 5c′). Modifying these parameters resulted in a satisfactory spectrum for Zn^{II}-**BIAIP**, as shown in Figure 5b′. Magnetic parameters for N1′-(amino) and N3′ (imino) were neglected according to their small size as reported by Kim et al.[35,90] The EPR parameters obtained from the spectrum simulations are listed in Table 2.

DFT Calculations. For detailed vibrational assignments, DFT calculations were worked out. The theoretical calculations for characterizing a phenoxyl radical are not trivial due to its strong interaction with a solvent and the difficulty of accounting for electronic correlation.[91−93] However, DFT methods are generally able to correctly describe the trends, despite some variations in reported computational results.[94−98] The B3LYP functional reportedly provides reliable results for geometry as well as vibrational frequencies,[93,94,96,98] and hence we used this to obtain geometrical characteristics and to corroborate the assignments of observed Raman bands.

The selected geometrical parameters in optimized structures are calculated from the DFT method for phenolic hydroxyl protonated (−OH), deprotonated ($-O^-$), and radical (−O•)

Scheme 1

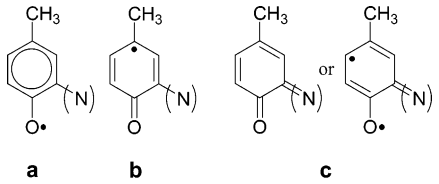

forms of M-**BIAIP** (M = Cu^{II}, Zn^{II}), Im-Ph, and *p*-cresol, respectively (Table S1, Supporting Information). The atomic Cartesian coordinates for all species are tabulated in Table S2−S5 (see Supporting Information). The optimized structure of *p*-cresol, which is within a category of the benzenoid structure shown in Scheme 1a, is very close to the geometry obtained from X-ray diffraction studies and DFT calculations.[96,99] Regarding *p*-cresolate and *p*-cresol, the structures display the contribution of a quinoidal form (Scheme 1b), in which C4−O, C2−C3, C5−C6, and Me−C1 are shorten concomitantly with the elongation of C1−C2, C3−C4, C4−C5, and C6−C1, respectively. Such calculated results are expected from the previous experimental and theoretical studies.[64,94−96,98]

For the −OH form of Im-Ph, the calculated C3−N1′ bond distance and the dihedral angle between the phenol and imidazole rings are comparable with the experimental values,[36,100] whereas relatively large variations exist for enzymes (C3−N1′ bond distance: 1.36,[12] 2.66,[11] and 1.43 Å;[13] Tyr-His dihedral angle: 44,[12] 66,[11] and 57°[13]). By introducing imidazole at the ortho position of the cross-linked phenol, the bond distance for the phenol ring became asymmetric with respect to the C_2 axis (which passes through C−O and C−Me bonds), as seen for M^{II}-**BIAIP** and Im-Ph. Such structural perturbation can be explained in terms of the resonance structure shown in Scheme 1c, whose contribution turns out to be larger for the radical forms. Both the notable decreases in the C4−O bond distance and the relatively small dihedral angle between the two rings can also be interpreted in terms of the contribution of the canonical structure in Scheme 1c to the radical form of M^{II}-**BIAIP** and Im-Ph in comparison with *p*-cresol. Moreover, the C3−N1′ bonds of the radical form were shorter than those of the −OH forms, and the dihedral angles between the phenol and imidazole rings decrease to nearly half that of the −OH forms for the radical form. These trends are consistent with previous reports.[35,96]

The calculated M^{II}-N(Im) distances did not change dramatically upon the deprotonation and one-electron oxidation of the phenol moiety, with all of the distances being within the values of Cu^{II}-N(Im or pyridyl) (1.966∼2.581 Å) revealed by X-ray crystallography.[31,101−103] On the other hand, the bonds of M^{II}-N(amino) were calculated to be longer than the experimental values of Cu^{II}-N (1.941∼2.145 Å),[31,101−103] suggesting very weak interactions between these atoms.

(87) Itoh, S.; Taki, M.; Kumei, H.; Takayama, S.; Nagatomo, S.; Kitagawa, T.; Sakurada, N.; Arakawa, R.; Fukuzumi, S. *Inorg. Chem.* **2000**, *39*, 3708−3711.
(88) Shimazaki, Y.; Huth, S.; Hirota, S.; Yamauchi, O. *Inorg. Chim. Acta* **2002**, *331*, 168−177.
(89) Hoganson, C. W.; Babcock, G. T. *Biochemistry* **1992**, *31*, 11874−11880.
(90) Although nitorogen hyperfine splittings can hardly alter the spectral pattern as well as peak positions, those seem to affect the line width slightly.
(91) Tripathi, G. N. R. *J. Phys. Chem. A* **1998**, *102*, 2388−2397.
(92) Chipman, D. M.; Liu, R.; Zhou, X.; Pulay, P. *J. Chem. Phys.* **1994**, *100*, 5023−5035.
(93) Qin, Y.; Wheeler, R. A. *J. Chem. Phys.* **1995**, *102*, 1689−1698.
(94) Qin, Y.; Wheeler, R. A. *J. Am. Chem. Soc.* **1995**, *117*, 6083−6092.
(95) Nwobi, O.; Higgins, J.; Zhou, X.; Liu, R. *Chem. Phys. Lett.* **1997**, *272*, 155−161.
(96) Bu, Y.; Cukier, R. I. *J. Phys. Chem. B* **2005**, *109*, 22013−22026.
(97) We will not discuss the spin density distribution calculated with B3LYP because of the limitation pointed out by Qin and Wheeler in ref 93.
(98) Schnepf, R.; Sokolowski, A.; Müller, J.; Bachler, V.; Wieghardt, K.; Hildebrandt, P. *J. Am. Chem. Soc.* **1998**, *120*, 2352−2364.
(99) Bois, P. C. *Acta Crystallogr.* **1970**, *B26*, 2086−2093.
(100) Naruta, Y.; Tachi, Y.; Chishiro, T.; Shimazaki, Y.; Tani, F. *Acta Crystallogr.* **2001,** E57, o550-o552.
(101) Bernarducci, E.; Bharadwaj, P. K.; Krogh-Jespersen, K.; Potenza, J. A.; Schugar, H. J. *J. Am. Chem. Soc.* **1983**, *105*, 3860−3866.
(102) Nagao, H.; Komeda, N.; Mukaida, M.; Suzuki, M.; Tanaka, K. *Inorg. Chem.* **1996**, *35*, 6809−6815.
(103) Relative insensitivity of phenol form to Cu^{II}-N seems to consistent with the unchanged Cu_B-CO vibrational frequency at various pH (pD) observed for cytochrome ba_3 oxidase from Thermus thermophilus in ref 118 and 119, although contradictory results have been reported for aa_3 cytochrome *c* oxidase from *Rhodobacter sphaeroides* in ref 120−123.

Table 3. Calculated (B3LYP/6-31G*) and Observed Vibrational Frequencies (ν/cm^{-1}) for Im-PhO• [2-(1-imidazoyl)-4-methylphenoxyl][a]

N. A.		^{18}O				ImD3[b]				CrD6[c]				
calc	obs	calc	Δ_{calc}[e]	obs	Δ_{obs}[e]	calc	Δ_{calc}	obs	Δ_{obs}	calc	Δ_{calc}	obs	Δ_{obs}	assignment[d]
1635	1587	1634	−1	1587	0	1635	0	1587	0	1598	−37	1557	−30	8a (C−C str)
1553	1530	1543	−10	1508	−22	1552	−1	1530[f]	0[f]	1539	−14	1520	−10	7a′(C−O str)
1500	1488	1500	0			1499	−1			1480	−20	1435	−53	19b + C3−N1'st
1484	1449	1481	−3	1449	0	1487	+3	1449	0	1460	−24	1420	−29	8b
1455	1409	1447	−8	1402	−7	1449	−6	1409[f]	0[f]	1371	−84	1354	−55	19a
1411	1366	1410	−1	1366	0	1399	−12	1354[f]	0[f]	1332	−79	1310	−56	14 + Im
1352	1315	1352	0	1315	0	1285	−67							Im + 14
1318	1290	1318	0	1290	0	1318	0			1254	−64			3
1286	1262	1285	−1	1262	0	1082	−204			1287	+1			Im CH bend
1237		1237	0			1228	−9			902	−335			9a
1221		1221	0			1216	−5			1175	−46			7a

[a] Observed frequencies are quoted from ref 34. [b] 2-(1-[2′,4′,5′-d$_3$]imidazoyl)-4-methylphenoxyl. [c] 2-(1-imidazoyl)-4-[d$_3$]methyl[d$_3$]phenoxyl. [d] Wilson-mode descriptions for the phenols; see refs 63, 98, and 104 for further details. [e] $\nu_{isotope} - \nu_{N.A.}$ [f] The precise values were not reported.

Both C4−O and C2−C3 (C5−C6) bond distances are good indicators of the contribution of a quinoidal structure (Scheme 1b). As far as the radical forms are concerned, the C4−O bond is shortened in the order of *p*-cresol (1.257 Å) > Im-Ph (1.252 Å) > M^{II}-**BIAIP** (1.251 Å), whereas the lengths of the C2−C3 (C5−C6) bonds were in the following order: Im-Ph (1.381 Å) > M^{II}-**BIAIP** (1.377 Å) > *p*-cresol (1.376 Å), based on a comparison of the average values relative to the C_2 axis. Therefore, judging from the optimized structure, in comparison with *p*-cresol we can expect an upshift of the Raman frequencies for 7a′ (C−O stretching) and a downshift of the 8a (C−C stretching) mode of **BIAIP**s and Im-Ph. Moreover, the spin densities at O and C3 (C5) positions would decrease when the C4−O and C2−C3 (C5−C6) bonds are shorten, respectively (Schnepf et al.).[98] The actual vibrational frequency calculation produces upshifts for both 8a and 7a′, with those computational results being consistent with the experimental ones (Table 1). To discuss the validity and the limitation of DFT methods, these predictions from the DFT calculation are compared with the experimental results in the section entitled "Interpretation of UVRR Spectra".

To assign Raman bands and reveal the construction of normal modes, the isotope shifts were calculated for Im-PhO• (Table 3). The Wilson-mode notation was used to describe the phenol modes.[63,98,104] The unscaled values are listed according to Qin and Wheeler,[93] and the observed frequencies were taken from Aki et al.[34] The discrepancy between the calculated and observed frequencies is not improved dramatically when using a single scaling. However, the order of the normal-mode frequencies and the sizes of isotope shifts appear to exhibit the observed trends. The obtained normal modes essentially represent those of a mixture of the phenol and imidazole modes as suggested previously.[34] The isotope shifts for 2-(1-imidazoyl)-4-[d$_3$]-methyl[d$_3$]phenoxyl are so large that the construction of the normal modes would also be influenced. For 2-(1-[2′,4′,5′-d$_3$]-imidazoyl)-4-methylphenoxyl, the difference spectrum in Figure 5 of ref 34 shows clear differential patterns for 1530-cm^{-1} (7a′), 1409-cm^{-1} (19a), and 1366-cm^{-1} (14) bands, indicating small downshifts upon deuterium labeling for these modes. Thus, calculating the frequencies using DFT in combination with isotope shifts is sufficiently reliable for assigning the observed bands, even for the radical form of Im-PhO•. Most of the observed Raman bands were mainly assigned to the phenol modes, taking the isotope shifts into account. The enhancements of modes 19b and 8b, which are not observed for *p*-cresol, apparently result from the cross-linkage with imidazole.

The Mulliken atomic spin densities calculated by DFT suggest that the spins are mainly localized on the phenol moiety, where these densities on the phenol rings are 0.964, 0.966, and 0.917 for the radical forms of Cu^{II}-**BIAIP**, Zn^{II}-**BIAIP**, and Im-PhO•, respectively. The slightly smaller spin for Im-PhO• is probably attributable to the smaller optimized dihedral angle between the phenol and imidazole planes, which is 31, 32, and 24° for Cu^{II}-**BIAIP**, Zn^{II}-**BIAIP**, and Im-PhO•, respectively.

Discussion

Interpretation of UVRR Spectra. The establishment of UVRR spectrum for the phenoxyl radical and its band assignment are the main purpose of this study in relation to interpretation of UVRR spectrum of the P intermediate of cytochrome *c* oxidase. Table 1 compares the calculated Raman frequencies for the phenoxyl radicals of **BIAIP**s, Im-Ph, and *p*-cresol with the observed ones. As mentioned above for Im-Ph, the mixing of phenol modes of **BIAIP**s with the cross-linked imidazole modes is anticipated by symmetry reduction, and extensive mixing occurred for frequencies lower than 1300 cm^{-1}. For example, such mixing resulted in the interchange of the absolute frequency relation between 7a and 9a. The very weak 7a and 9a band intensities in our UVRR spectra are presumably due to the dispersion of Raman enhancement over a range arising from extensive mixing with imidazole modes. Most of the frequency shifts of phenol modes of **BIAIP**s and Im-Ph compared with those of *p*-cresol can be understood in terms of a structural perturbation and a local mode mixing caused by the introduction of imidazole. Although the mixings produced significant effects, a better separation between cross-linked and non-cross-linked imidazoles was evident.

Previous studies have classified the frequencies of 8a (C−C stretching) and 7a′ (C−O stretching) into two types: the phenoxyl type (8a: 1552−1577 cm^{-1}, 7a′: 1502−1517 cm^{-1}) and the *p*-benzosemiquinone-anion type (8a: 1636 and 1620 cm^{-1}, 7a′: 1434 and 1435 cm^{-1}).[105−107] The phenoxyl-type 8a and 7a′ bands are normally weak and strong in intensity, respectively, which is opposite to those for the *p*-benzosemiquinone-anion type. For **BIAIP**s and Im-Ph, 8a and 7a′ were

(104) Varsányi, G. *Assignment for vibrational spectra of seven hundred benzene derivatives*; Adam Hilger: London, 1974; Vol. 1, p 323.

(105) Tripathi, G. N. R.; Schuler, R. H. *J. Phys. Chem.* **1988**, *92*, 5129−5133.
(106) Tripathi, G. N. R.; Schuler, R. H. *J. Phys. Chem.* **1987**, *91*, 5881−5885.
(107) Tripathi, G. N. R.; Schuler, R. H. *J. Phys. Chem.* **1984**, *88*, 1706−1710.

Scheme 2

$$I_P \xleftarrow[\sigma_P]{\nu} P \xrightarrow[\sigma_A]{\nu} T \xrightarrow[\sigma_T]{\nu} I_T$$

observed in the frequencies intermediate to the phenoxyl and *p*-benzosemiquinone-anion type (Table 1), whereas the intensity distribution of the Raman bands was close to that of the *p*-benzosemiquinone-anion type.

Shorter bonds and higher vibrational frequencies for **BIAIP**s and Im-Ph than for *p*-cresol as calculated by DFT suggest a frequency upshift of 7a′ compared with that of *p*-cresol. Indeed, such upshifts of ca. 15 cm^{-1} were observed experimentally. Layton et al. reported an empirical rule for the correlation between bond lengths and stretching frequencies for C−O.[108] The following relation is obtained from a linear fit by taking their listed data for less than the frequency of 1830 cm^{-1}:

$$(\text{C-O distance/Å}) = -2.99 \times 10^{-4} \times (\text{C-O frequency/cm}^{-1}) + 1.73 \quad (2)$$

The plots of the observed values are given in Figure S9 (see Supporting Information). With eq 2, a difference of 0.6 Å results in a frequency shift of 20 cm^{-1} for BIAIPs compared with *p*-cresol, which is comparable with the experimental value. Upon the substitution of phenol oxygen with ^{18}O, both 7a′ and 19a show the isotope shifts for Im-Ph, confirming the assignment. Thus, the upshifts of 7a′ and 19a in BIAIPs are attributed to shortening of the C−O bond. Upshifts of 8a for **BIAIP**s and Im-Ph were also observed, in contrast to the expectation of downshifts based on the optimized C2−C3 (C5−C6) bond distances calculated by DFT. The calculated normal mode suggests that an imidazole mode (C4′-C5′ stretching) is located in the proximity of 8a, with the resulting vibrational mixing being responsible for the observed upshift of 8a.

Observed Raman frequencies as well as DFT calculations suggest the moderate delocalization of π electrons between phenol and imidazole rings, which causes the upshifts of 8a, 7a′ and 19a for the phenoxyl radical form of **BIAIP**s.

Saturation Effect. Dependency of Raman intensities on laser intensities was not self-evident. Therefore, we analyzed the laser-intensity dependency of the Raman intensity more quantitatively using the procedure of Johnson et al. (see Scheme 2),[62] where *P* and *T* are the precursor (phenolic hydroxyl deprotonated, in this case) and transient (phenoxyl radical) species, respectively; I_P and I_T denote the Raman intensities of *P* and *T*, respectively; and σ_A, σ_P, and σ_T are the cross sections for the photochemical reaction (photoelectron ejection) and the Raman scatterings from *P* and *T*, respectively. A process of single-photon electron release is assumed for the conversion from *P* to *T* in this model. According to the formulation by Johnson et al. with some modification,[62,109,110] the following relations are obtained:

$$\sigma_P = \frac{I_P}{I_S} \frac{\sigma_S C_S I_0}{\frac{P_0}{\sigma_A}\{1 - \exp(-\sigma_A I_0)\}} \left[\frac{\nu_0 - 981}{\nu_0 - \nu_P}\right]^4 \quad (3)$$

$$\sigma_T = \frac{I_T}{I_S} \frac{\sigma_S C_S}{P_0\left[1 + \frac{1}{\sigma_A I_0}\{\exp(-\sigma_A I_0) - 1\}\right]} \left[\frac{\nu_0 - 981}{\nu_0 - \nu_T}\right]^4 \quad (4)$$

where I_0 is the total light intensity integrated over a single pulse, P_0 is the initial concentration of *P*, and I_S, C_S, and σ_S are the Raman intensity, concentration, and Raman scattering cross section of the 981-cm^{-1} band of the internal standard (SO_4^{2-}), respectively. The value of σ_S was fixed at 0.385 millibarn $molecule^{-1}$ $steradian^{-1}$ for the analyses.[41,111] eqs 3 and 4 are employed for the data sets of the parent and radical species, respectively. In this analysis, the values of σ_P were set to those obtained previously.[41] The estimated cross sections for the selected Raman bands of phenoxyl radicals (σ_T) are tabulated in Table 4. The estimated cross sections for Zn^{II}-**BIAIP** and *p*-cresol do not differ dramatically, implying that *both imidazole-phenol cross-linkage and Zn^{II} coordination to N3′ of imidazole have little effect on the electronic structure of the phenoxyl radical form of Zn^{II}-**BIAIP***.

Spin Density Distribution. To understand the Raman changes of individual stretching frequencies upon radical formation of BIAIP, it is very helpful to see spin density distribution in the radical form. A hyperfine interaction comprises isotropic and anisotropic parts. For the isotropic hyperfine part, which arises from Fermi contact interaction, the hyperfine interaction of the α-proton ($A^{H\alpha_{iso}}$) is proportional to the spin density at the bonded carbon atom, which is the so-called McConnell relation ($A^{H\alpha_{iso}} = Q\rho_C$).[54] Such a proportional relationship is approximately valid for the anisotropic part of the α-proton hyperfine interaction ($A^{H\alpha_{aniso}}$), which originates from dipole−dipole interactions between the electron and the nuclear spins. A similar equation also applies to the hyperfine splitting of methyl β-proton ($A^{H\beta}$), which is proportional to the spin density on the carbon atom bonded to the methyl group (C1).[54,89,112] This hyperfine interaction of the β-proton is almost isotropic but depends on the dihedral angle between the C−H and principal axis of the π orbital because it originates from hyperconjugation. However, the three protons of the methyl group become equivalent at 77 K due to its fast internal rotation.[35] We can estimate the spin density distribution at each carbon using the proportionality of hyperfine splitting to spin density, as shown in Figure 6.

The spin densities at C1, C2 (C6), and C5 positions are estimated to be 0.29, −0.04, and 0.18, respectively, for the phenoxyl radical form of Zn^{II}-**BIAIP**. The influence of the imidazole substituent on the electronic structure of the phenoxyl radical is so small that the difference of the spin density for the phenol moiety between Zn^{II}-**BIAIP** and *p*-cresol is at most 0.1, which is supported by the DFT calculations described here. Our EPR result is consistent with those from an ESEEM study.[35] The slight decrease of the spin density at the ortho carbon (C5) appears to arise from the flow out of the spin into the imidazole moiety rather than the contribution of a quinoidal structure (Scheme 1b).

Role of Tyr-His-Cu_B Unit. To understand the role of covalent linkage in the Tyr-His-Cu_B group, it is required to

(108) Layton, J., E. M.; Kross, R. D.; Fassel, V. A. *J. Phys. Chem.* **1956**, *25*, 135−138.
(109) El-Mashtoly, S. F.; Yamauchi, S.; Kumauchi, M.; Hamada, N.; Tokunaga, F.; Unno, M. *J. Phys. Chem. B* **2005**, *109*, 23666−23673.
(110) Wen, Z. Q.; Thomas, G. J. *Biopolymers* **1998**, *45*, 247−256.
(111) Dudic, J. M.; Johnson, C. R.; Asher, S. A. *J. Chem. Phys.* **1985**, *82*, 1732−1740.
(112) Budiman, K.; Kannt, A.; Lyubenova, S.; Richter, O. M.; Ludwig, B.; Michel, H.; MacMillan, F. *Biochemistry* **2004**, *43*, 11709−11716.

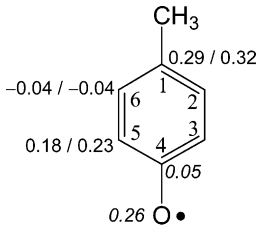

Zn^{II}-**BIAIP** / *p*-cresoxyl

Figure 6. Spin-density distribution estimated for the radical form of Zn^{II}-**BIAIP** and *p*-cresol. Italic numbers are the spin densities reported previously.[54]

Table 4. Cross-Section σ_T (millibarn/(molecule•Steradian)) Values for Selected Raman Bands of Phenoxyl Radicals

	8a	7a′	19a
Zn^{II}-**BIAIP**	22	5.6	11
p-cresol	31	49	20

integrate the individual spectroscopic observations. The pH dependencies of absorption spectra and the results of DFT calculations suggest that the interaction between Cu^{II} and N8′ is negligible for Cu^{II}-**BIAIP**. Thus, the present model reproduces a similar coordination environment to that of the Cu_B site of the enzyme. Our experimental results also reveal that the pK_a value of phenolic OH of Cu^{II}-**BIAIP** (9.8) is nearly the same as that of *p*-cresol (10.2). This similarity is compatible with the cross-linked tyrosine OH being protonated in the oxidized form when the pH is between 7.4 and 8.5 (Kandori et al.[113]), and in the oxidized and reduced form for a pH lower than 9 (Iwaki et al.[114−117]) based on FT-IR experimental results, in contrast with the proposal of Yoshikawa et al.[12] The conservation of the Cu^{II} environment as well as phenolic OH protonation for Cu^{II}-**BIAIP** for pH values between 5 and 10 is consistent with no change in the Cu_BC−O frequency being observed for pH values between 5.5 and 9.7 for CO-bound cytochrome ba_3 from *Thermus thermophilus*, whereas the interpretation of the pH dependencies of Fe^{II}-CO, Fe^{II}C−O, and Cu^{I}C−O is still controversial.[118−122] In other words, a role of proton delivery is unlikely for cross-linked phenol except when proton release is coupled with one-electron oxidation, because the pK_a of the protonated phenoxyl radical form is remarkably low.

We have assigned the observed Raman bands and elucidated the vibrational frequencies of some cross-linked phenoxyl modes (8a, 7a′, 19b, 8b, 19a, and 14) with the help of DFT calculations. The observed frequencies of **BIAIP**s well correspond to those of Im-Ph, and hence the obtained frequency shifts of phenoxyl-radical modes relative to *p*-cresol are concluded to be inherent in the imidazole-phenol unit. The upshift of 7a′ (C−O stretching) by ca. 15 cm^{-1} is especially significant, suggesting that band assignments should be revised given the differential FT-IR spectra observed for enzymes.[113−117,123]

Both transient absorption and EPR results suggest that the effect of the imidazole-phenol covalent-linkage on the electronic structure of the phenoxyl radical is smaller than expected. Thus, we can speculate that the redox potential would not be dramatically changed even for cross-linked phenol. The possibility of its putative role as the source of the fourth electron is less likely from our transient absorption and EPR results, although the failure of the EPR-based detection of the radical form of Cu^{II}-**BIAIP** seems to corroborate the EPR-silent character of Tyr244 (the residue number is based on bovine enzyme).[112] The weak phenoxyl radical signals in all of our experiments also make H-atom transfer from the Tyr244 hydroxyl group to dioxygen during the reduction indeterminable, because both the one-electron oxidation followed by proton release and the H-atom transfer should generate the same product (i.e., the phenoxyl radical). The processes of electron transfer followed by a proton transfer are too fast to separate using our setup for measuring the transient absorption, which has a temporal resolution of ca. 40 ns.[53] To verify the spectroscopic character of the Tyr-His-Cu_B unit further, the introduction of a protected group at the ortho position of the phenol ring (as described by Kim et al.[30] and Kamaraj et al.[31]) would be appropriate for reducing the reactivity of a phenoxyl radical.

Consequently, the most likely role of the Tyr-His-Cu_B unit is that it retains the polar structure of the Cu_B site, which has been proposed by Das et al.[17] and Pinakoulaki et al.,[15] or that it fixes a water molecule in the proximity of the binuclear center, rather than that it provides the fourth electron to oxygen. Both of them will significantly contribute to H^+ transfer, instead of H-atom one, to the heme-bound dioxygen. The latter is supported by a study[28] that investigated a chemical model bearing all related groups around a heme: at an early stage of the oxygenation, the corresponding superoxy species was remarkably stabilized in the presence of water molecules, presumably through hydrogen bonds between the phenolic OH and the bound O_2.

Conclusions

The aim of this study was to elucidate the role of the Tyr-His-Cu_B unit in the enzyme by examining the physicochemical properties of its model compounds M-**BIAIP** (M = Cu^{II}, Zn^{II}). The following conclusions can be drawn from our investigations:

(1) Phenolic hydroxyl (p$K_a \approx 10$) is protonated for the parent Cu^{II}-**BIAIP** at physiological pH.

(2) The main phenoxyl modes (8a, 7a′, and 19a) of **BIAIP**s observed by UVRR are upshifted as the consequence of the imidazole-phenol cross-linkage.

(3) The effect of the Tyr-His-Cu_B^{II} unit on the electronic structure of the radical form is minor, as confirmed by transient absorption measurements, EPR spectroscopy, and DFT calculations.

(4) The cross-linked tyroxyl radical is expected to be EPR-silent due to magnetic coupling with Cu_B^{II}.

(113) Kandori, H.; Nakamura, H.; Yamazaki, Y.; Mogi, T. *J. Biol. Chem.* **2005**, *280*, 32821−32826.
(114) Iwaki, M.; Puustinen, A.; Wikström, M.; Rich, P. R. *Biochemistry* **2004**, *43*, 14370−14378.
(115) Iwaki, M.; Puustinen, A.; Wikström, M.; Rich, P. R. *Biochemistry* **2003**, *42*, 8809−8817.
(116) Iwaki, M.; Breton, J.; Rich, P. R. *Biochim. Biophys. Acta* **2002**, *1555*, 116−121.
(117) Iwaki, M.; Rich, P. R. *J. Am. Chem. Soc.* **2004**, *126*, 2386−2389.
(118) Koutsoupakis, K.; Stavrakis, S.; Pinakoulaki, E.; Soulimane, T.; Varotsis, C. *J. Biol. Chem.* **2002**, *277*, 32860−32866.
(119) Koutsoupakis, K.; Stavrakis, S.; Soulimane, T.; Varotsis, C. *J. Biol. Chem.* **2003**, *278*, 14893−14896.
(120) Das, T. K.; Tomson, F. L.; Gennis, R. B.; Gordon, M.; Rousseau, D. L. *Biophys. J.* **2001**, *80*, 2039−2045.
(121) Das, T. K.; Gomes, C. M.; Teixeira, M.; Rousseau, D. L. *Proc. Natl. Acad. Sci. U.S.A.* **1999**, *96*, 9591−9596.
(122) Mitchell, D. M.; Shapleigh, J. P.; Archer, A. M.; Alben, J. O.; Gennis, R. B. *Biochemistry* **1996**, *35*, 9446−9450.
(123) Nyquist, R. M.; Heitbrink, D.; Bolwien, C.; Gennis, R. B.; Heberle, J. *Proc. Natl. Acad. Sci. U.S.A.* **2003**, *100*, 8715−8720.

(5) The role of the Tyr-His-Cu_B unit in the enzyme is probably to retain a polar binuclear site so as to allow heterolytic cleavage of the O−O bond or fixing of a water molecule near O_2 by mediation of H^+ transfer, unless a dramatic change of redox potential or the reduction of the dihedral angle occurs within the imidazole-phenol unit.

Acknowledgment. We thank Professor Yasuhiko Yamamoto and Dr. Shigenori Nagatomo of Tsukuba University for use of the UVRR instrument and Professor Kimio Akiyama and Mr. Satoru Nakajima of Tohoku University for their help in performing the EPR experiments under UV irradiation and in measuring the transient absorption spectra. We also thank the Research Center for Computational Science of this institute for the use of the SGI Origin2000, SGI2800, Origin3800, and NEC TX7 computers and the Instrument Center of this institute for use of an EPR machine. This study was supported by JSPS Research Fellowships for Young Scientists to Y.N. (Okazaki) and for Foreign Researchers to J.-G.L., by Grants-in-Aid for Specifically Promoted Research (14001004) from the Ministry of Education, Culture, Sports, Science and Technology, Japan, to T.K., and for Scientific Research (A) (14204073)/(S)(17105003) to Y.N. (Kyusyu University).

Supporting Information Available: (1) Transient absorption of 2,4,6-tri-*tert*-butylphenol, (2) pH dependency of *p*-cresol absorption spectra and of Cu^{II}-BIAIP absorption spectra, (3) Laser-intensity dependency of the Raman intensities of *p*-cresolate and *p*-cresoxyl radical, of the Raman intensities of Zn^{II}-BIAIP, of the UVRR spectra of *p*-cresolate and *p*-cresoxyl radical, and of the UVRR spectra of Zn^{II}-BIAIP, (4) Observed and simulated EPR spectra of the Cu^{II}-BIAIP parent molecule, (5) Correlation plot of C−O distance vs C−O frequency, (6) Optimized geometry obtained by DFT calculations, and (7) Selected vibrational frequencies and assignments for phenoxyl radicals. This material is available free of charge via the Internet at http://pubs.acs.org.

JA061507Y